Aerosol Science and Technology 31:275–285 (1999)

Published by Taylor and Francis
0278-6826 /99 /$12.00 +.00

Concentration Effect of Chromic Acid Solutions on the Enrichment of Cr(VI) in Droplets from Bursting Bubbles

Yu-Mei Kuo and Chiu-Sen Wang
GRADUATE INSTITUTE OF ENVIRONMENTAL HEALTH, NATIONAL TAIWAN UNIVERSITY, ROOM 1505, NO. 1, JEN-AI ROAD, SEC. 1, TAIPEI, TAIWAN

ABSTRACT. The effect of electrolyte concentration on the enrichment of Cr(VI) in droplets generated from bubbles bursting on the surface of chromic acid solution was investigated with an experimental bubbling system for CrO_3 concentrations in the range of 31.25–375 g / L in the bulk solution with a gas flow rate of 4 L / min. A cascade impactor collected droplet samples on polyvinyl chloride filters for chemical analysis. A laser aerosol spectrometer and an aerodynamic particle sizer were employed simultaneously to measure the number concentration and size distribution of the droplets. For the 5 electrolyte concentrations studied, the measured droplet size distributions had count median diameters (CMDs) in the range of 0.15–0.18 μm. The droplet volume distributions calculated from droplet number concentration data were bimodal, indicating the presence of both film and jet droplets which had a mode at 3–4 μm and over 10 μm, respectively. As the CrO_3 concentration in the bulk solution increased, the mode of the volume distribution of film droplets tended to shift toward smaller sizes, whereas that of jet droplets tended to shift toward larger sizes. The concentration ratio, defined as the ratio of the Cr(VI) concentration in droplets to that of the bulk solution, was found to decline sharply with increasing electrolyte concentration in the bulk solution.

INTRODUCTION

In the process of chromium electroplating, oxygen and hydrogen gases evolve at the electrodes and thereby give rise to the formation of gas bubbles in the electrolyte solution. The gas bubble rises to the liquid surface, forms a hemispheric film cap, and then bursts. As a result, droplets containing chromium are formed. Droplets generated in chromium electroplating processes have received considerable attention in Taiwan because of high prevalence rates of nasal septum ulcers or perforations among workers (Lin et al. 1994).

The generation of droplets from bursting of single bubbles involves 2 distinct mechanisms: film breakage and jet formation. When a gas bubble produced in the bulk of an electrolyte solution rises to the liquid surface, it forms a hemispheric film cap above the surface. The film cap becomes thinner because of liquid drainage and

breaks into numerous droplets in a wide range of sizes when its thickness reaches a certain critical value. The droplets, named film droplets, vary from submicrometer to 20 μm in diameter (Garner et al. 1954). Immediately following the breakage of a bubble, the surrounding liquid fills the remaining bubble cavity and a liquid jet appears in the center of the crater. Jet droplets are produced from breakup of the jet rising upward from the collapsing bubble cavity. In general, jet droplets are about 10 times larger than film droplets (Newitt et al. 1954).

Information on the characteristics of droplets is needed in the assessment of health effects and the control of chromium emission. Compounds containing Cr(VI) are highly toxic and carcinogenic. In addition to the chemical property of droplets, the droplet size is important in assessing health effects because the droplet size influences the sites where the droplets deposit in the respiratory system. Droplets formed by bursting bubbles tend to be enriched with certain species in the solution. Previous studies found an enrichment of trace metal such as Zn, Cu, and Fe relative to Na in the oceanic droplets generated from bursting bubbles (Van Grieken et al. 1974; Piotrowicz et al. 1979). Similarly, results of a study at an electroplating plant showed that the chromate tended to be enriched relative to sulfate in droplets in the size range of 3 to 7 μm (Rondia and Closset 1985).

This study was aimed at evaluating the concentration effect of chromic acid solutions on the enrichment of Cr(VI) in droplets released from bubbles bursting on the surface in an experimental system.

METHODS

The Experimental System

Figure 1 shows a schematic diagram of the experimental system. The apparatus consisted of a glass cylindrical tank, a water

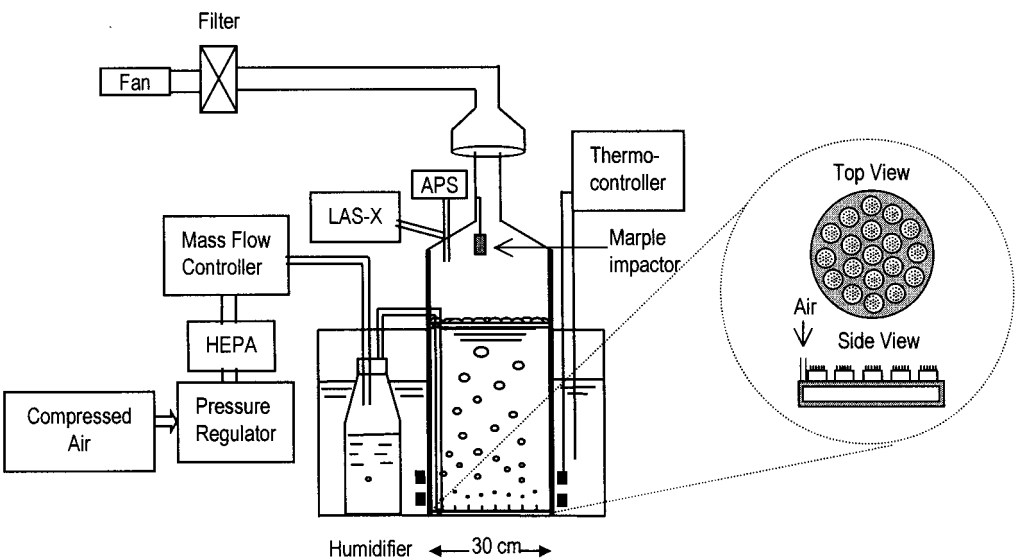

FIGURE 1. A schematic diagram of the experimental system.

bath, a bubbling system, and the droplet sampling/measuring instruments. The cylindrical tank, 30 cm in diameter, was sufficiently large so that the wall effect on the size of bubbles being produced can be neglected. The tank was put in a water bath to maintain the liquid temperature in the tank where it would be in an electroplating tank. In this study, the liquid temperature and the air temperature in the chamber above the solution were kept at 45 and 37°C, respectively. Measurements indicated that the relative humidity of the air inside the tank was over 99% during the experiments.

The bubbling system consisted of 19 circular caps, each containing 19 glass capillaries of 0.2 mm in inner diameter and 3.2 cm in length. The system was similar to those used by Wangwongwatana et al. (1990) and by Pilacinski et al. (1990). Sparging air through the CrO_3 solution in the tank led to formation of droplets above the liquid surface. The sparging air was obtained from a laboratory air supply and its flow rate was controlled by a mass flow controller. The air passed through a HEPA filter and a humidifier before entering the bubbling system.

The Sampling System

To measure the Cr(VI) concentration in droplets, a Marple personal cascade impactor (Model 290, Graseby Andersen, Atlanta, GA, U.S.A.) was used to collect droplets on polyvinyl chloride filters (PVC filters, 34 mm, 5 μm pore size, Omega Specialty Instrument Co., Chelmsford, MA, U.S.A.). The impactor had 8 stages with aerodynamic cutoff diameters of 0.6, 1, 1.5, 3.5, 6, 10, 15, and 21 μm at a sampling flow rate of 2 L/min. Droplets of various size ranges were collected on PVC filters, and the Cr(VI) concentrations in the samples were determined by chemical analysis. The impactor was placed at 35 cm above the liquid surface.

Two real-time aerosol instruments, a laser aerosol spectrometer (Model LAS-X, Particle Measuring Systems Inc., Boulder, CO, U.S.A.) and an aerodynamic particle sizer (APS, Model 3310, TSI, St. Paul, MN, U.S.A.), were employed to determine the size distribution of droplets which had a broad size range covering the sizes of both film and jet droplets. The aerosol sampling flow rates of a LAS-X and an APS were 0.3 and 1 L/min, respectively. The sampling probes of these 2 instruments were placed side by side at the same height above the liquid surface as that of the impactor.

Sampling and Analysis of Cr(VI) Droplets

The predominant constituent in the chromium-electroplating bath is CrO_3, although there might be a small amount of additives (usually 1% sulfuric acid) used in the shop. In this study, only CrO_3 was added in the bath. Five concentrations of chromic acid solutions were used to conduct the experiments. Table 1 lists the physical properties of test solutions at 45°C and 1 atm. The density of the solution was determined by a weighing method while the surface tension and the viscosity were measured, respectively, by a tensionmeter (Model k12, Krüss, Hamburg, Germany) and a capillary viscometer (Ubbelohde Micro-viscometer,

TABLE 1. The physical properties of test solutions at 45°C and 1 atm.

CrO_3 concentration (g/L)	31.25	62.5	125	250	375
Density (g/cm^3)	1.021	1.044	1.087	1.177	1.265
Surface tension (dyne/cm)	65.15	65.93	66.97	68.23	69.55
Viscosity (g/cm s)	0.0062	0.0064	0.0064	0.0068	0.0074

capillary no. 5010a, Scott Geräte, Mainz, Germany).

For a given size of capillaries used for air sparging and given surface tension of liquids, the mean size of generated bubbles can be estimated by hydrostatic principles (see, for example, MaCann and Prince 1971). The estimated mean diameter of equivalent-volume bubbles ranged from 0.19–0.2 cm for chromic acid solutions of 31.25–375 g/L.

In each run, the electrolyte solution was first heated to 45°C in a storage container. Filtered and humidified air was then introduced into the bubbling system at a flow rate of 4 L/min, and the electrolyte solution was gradually transferred to the bubbling tank by a peristaltic pump (Model 505S, Watson Marlow, Falmouth, U.K.). Airborne droplets were sampled by an impactor for a duration of 2 h. The U.S. National Institute for Occupational Safety and Health (NIOSH) method 7600 was employed to determine the Cr(VI) concentration in each droplet sample. The method utilizes the reagent s-diphenylcarbazide, which reacts specifically with Cr(VI) to form a purple-red color complex. The absorbance by the color complex at 540 nm was measured using a spectrometer (UV-VIS recording spectrophotometer, Model UV-160A, Shimadzu Corporation, Japan). In each run, the number concentration and size distribution of the droplets were measured several times by an LAS-X and an APS simultaneously. Three runs were made for each electrolyte concentration.

RESULTS AND DISCUSSION

Effect of Electrolyte Concentration on the Number and Volume Concentrations of Droplets

To determine the droplet number concentration and size distribution, droplets in the range of 0.1–0.75 μm in optical diameter were measured by an LAS-X and those 0.75–30 μm in aerodynamic diameter were measured by an APS, simultaneously. The LAS-X utilizes a laser as a light source and detects the optical diameter of a particle. The APS measures the aerodynamic diameter by accelerating a particle through a nozzle and measuring the time it takes to pass 2 closely spaced laser beams.

Figure 2 compares the number distributions of droplets produced from various electrolyte concentrations. Although there was no sharp separation between film and jet droplets in the measured size distributions, droplets larger than 7 μm were presumably jet droplets, whereas those smaller than 7 μm were considered to be film droplets (the separation can be seen in both Figures 2 and 3). Figure 2 shows that the resulting droplets were mainly film droplets and the CMDs of film droplets were in the range of 0.15–0.18 μm. This finding is comparable to that reported by Resch and Aftei (1992), who found that the film droplets were mainly in the 0.05–0.3 μm range. Moreover, the estimated separating diameter of 7 μm is also comparable to the findings of Cirpriano and Blanchard (1981) and Woolf et al. (1987). These 2 papers reported, respectively, an estimated separating diameter of about 7.5 and 8 μm between film droplets and jet droplets.

The droplet number concentrations are shown in Table 2 for 5 different CrO_3 concentrations. The droplet number concentrations in the measured size range of 0.1–30 μm varied from 2 to 5×10^3 particles/cm^3 and the number concentration of film droplets was higher than that of jet droplets. The maximum number concentration of film droplets and jet droplets occurred at the CrO_3 concentrations of 125 and 62.5 g/L in the bulk solution, respectively. The number of concentration of jet

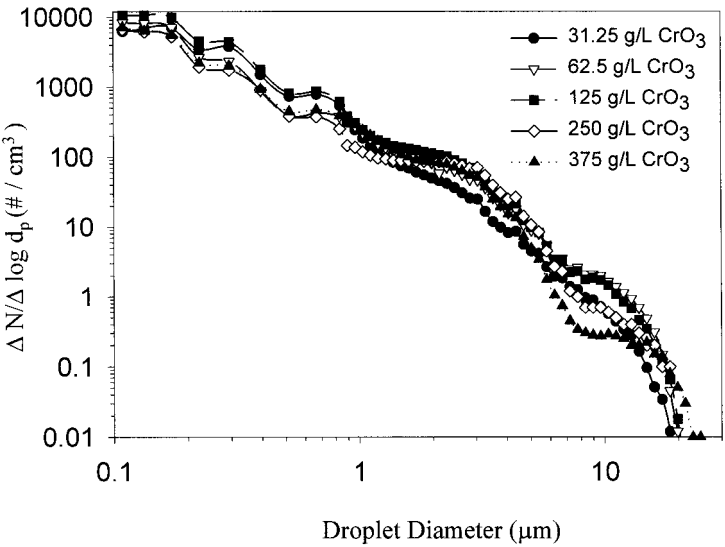

FIGURE 2. Comparison of droplet size distributions for CrO_3 concentrations of 31.25, 62.5, 125, 250, and 375 g/L. Aerodynamic diameter is used for > 0.75 μm, and optical diameter is used for < 0.75 μm.

TABLE 2. Summary of number concentrations, volume concentrations, and Cr(VI) mass concentrations in droplets generated from various concentrations of CrO_3 solution.

CrO_3 (g/L) in the bulk solution		31.25	62.5	125	250	375
Number concentration (#/cm^3)	0.1-7 μm	3335± 1282	3217± 1063	4680± 588	2470± 301	2659± 724
	> 7 μm	0.22± 0.07	0.57± 0.10	0.48± 0.17	0.22± 0.12	0.11± 0.02
Volume concentration ($\mu m^3/cm^3$)	0.1-7 μm	247± 35	399± 88	514± 50	464± 59	343± 119
	> 7 μm	108± 48	332± 52	266± 88	152± 96	104± 38
Cr (VI) concentration ($\mu g/m^3$)	0.6-7 μm	16.7± 0.7	30.2± 3.9	41.6± 5.7	52.9± 11.9	39.2± 8.0
	> 7 μm	15.9± 5.2	42.6± 5.0	32.8± 13.9	33.6± 12.6	19.3± 13.6

droplets decreased linearly as the electrolyte concentration increased, except for the lowest concentration of CrO_3 (31.25 g/L). However, it should be noted that droplets were increasingly undersampled with increasing droplet size because of the decreasing inlet efficiency of the APS.

The sampling efficiency of an APS with respect to particle size was investigated experimentally by Kinney and Pui (1995). The results showed that the APS sampled particles smaller than 10 μm with an efficiency of nearly 100%, whereas the efficiency dropped from around 80% for 20 μm particles to less than 60% for particles larger than 30 μm.

In this study, the data on droplet size distribution measured by the APS was not

corrected for the sampling efficiency of the APS. If the effect of undersampling for larger droplets was taken into account, the decreasing tendency of the jet droplet number concentration with increase in electrolyte concentration would be even more pronounced.

The sizing accuracy of an optical particle counter depends on the refractive index of the measured particles as well as that of the particles used for calibration. If the refractive index of CrO_3 droplets is assumed to be 1.333 (Washburn et al. 1930), a shift in size distribution measured by the LAS-X is expected. The effect of refractive index was studied theoretically by Hinds and Kraske (1986). According to their results, the LAS-X would underestimate the droplet sizes by 18 to 34% in the indicated size range of the present study.

Measured size distributions may be distorted by the coincidence effect of particles. The concentration for a coincidence error of 5% in the measurement with an APS for particles of 29 μm in diameter is 218 particles/cm^3. As for the LAS-X, there was less than a 1 channel width (average channel width is 10.6% of the lower limit) shift in the peak size for concentrations up to 10^4 particles/cm^3 (Hinds and Kraske 1986). In this study, the coincidence effect was acceptable because the number concentrations measured by an APS and an LAS-X were < 200 particles/cm^3 and in the order of 10^3 particles/cm^3, respectively.

In general, a sheath air system is employed in real-time aerosol measuring instruments to confine the aerosols. The sheath air of the APS came from a laboratory air supply with a relative humidity of about 10%. The low relative humidity of the sheath air might cause partial evaporation of sampled droplets. However, the residence time of droplets from the outlet of the inner nozzle to the sensing zone of the instrument is approximately a few tenths of a μs. In view of the evaporation time needed for particles of the size range detected by the APS, the influence of the sheath air on the size distribution was negligible. As for the LAS-X, the shifting of measured size distributions arising from changes in temperature and humidity of the sheath air was negligible because the LAS-X operated with a recirculated sheath air.

Figure 3 compares the droplet volume distribution calculated from number distribution data obtained for 5 CrO_3 concentrations studied. The droplet volume distributions were bimodal, indicating the presence of both film and jet droplets. The film droplet mode, in the range of 3–4 μm, shifted toward smaller sizes as the CrO_3 concentration increased, whereas the jet droplet mode, in the size range of 11–14 μm, shifted toward larger sizes with increasing CrO_3 concentrations. Exton et al. (1985) found a peak at about 4 μm in diameter in the volume spectrum of film droplets produced from seawater and our results are comparable to their finding. The observed shifting trend of the volume distribution mode of jet droplets is similar to that reported by Hinds and Kuo (1990). The number and size of jet droplets were functions of liquid viscosity. Fewer and larger jet droplets were generated from liquids of higher viscosities. However, with the limited results of this study it remains unclear why the volume distribution mode of film droplets shifted with respect to the electrolyte concentration.

Table 2 also shows the droplet volume concentrations in the measured size range of 0.1–30 μm for various CrO_3 concentrations. Similar to the maximum number concentration, the maximum volume concentration of film and jet droplets occurred at the CrO_3 concentration of 125 and 62.5 g/L in the bulk solution, respectively.

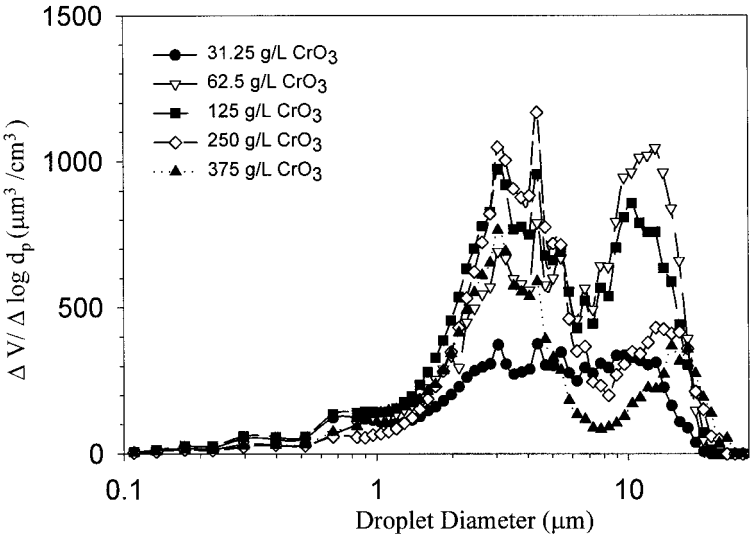

FIGURE 3. Comparison of droplet volume distributions for CrO_3 concentrations of 31.25, 62.5, 125, 250, and 375 g/L calculated from droplet number distribution data. Aerodynamic diameter is used for > 0.75 μm, and optical diameter is used for < 0.75 μm.

Effect of Electrolyte Concentration on Airborne Cr(VI) Concentration

Figure 4 presents the Cr(VI) mass distributions as well as droplet volume distributions for droplets larger than 0.6 μm in aerodynamic diameter determined by an impactor for CrO_3 concentrations of 31.25, 62.5, 125, 250, and 375 g/L. All the Cr(VI) mass distributions were bimodal with 1 peak around 3 to 4 μm and another at a diameter larger than 10 μm. The peak above 10 μm, which represented the contribution of jet droplets, moved to larger sizes as the CrO_3 concentration increased.

The sampling efficiency of the Marple personal impactor with respect to particle size has been experimentally investigated by Rubow et al. (1987) and Rader et al. (1991). An efficiency of nearly 100% was found for 10 μm particles, whereas the sampling efficiency decreased to about 80% for particles larger than 21 μm. Figure 4 shows that the shape of the Cr(VI) mass distribution was similar to that of the corresponding droplet volume distribution, except for the range larger than 10 μm where the APS gradually underestimated the droplet counts.

It can be seen in Table 2 that the airborne Cr(VI) mass concentration in droplets in the size range of 0.6–7 μm increased with increasing electrolyte concentration and reached a maximum, 52.9 $\mu g/m^3$, at the CrO_3 solution of 250 g/L in the bulk solution. In contrast, the maximum Cr(VI) mass concentration in jet droplets occurred at the CrO_3 concentration of 62.5 g/L in the bulk solution.

Cr(VI) Enrichment in the Droplets

During the bubbling process, droplets produced by bursting bubbles could be enriched with Cr(VI). The concentration ra-

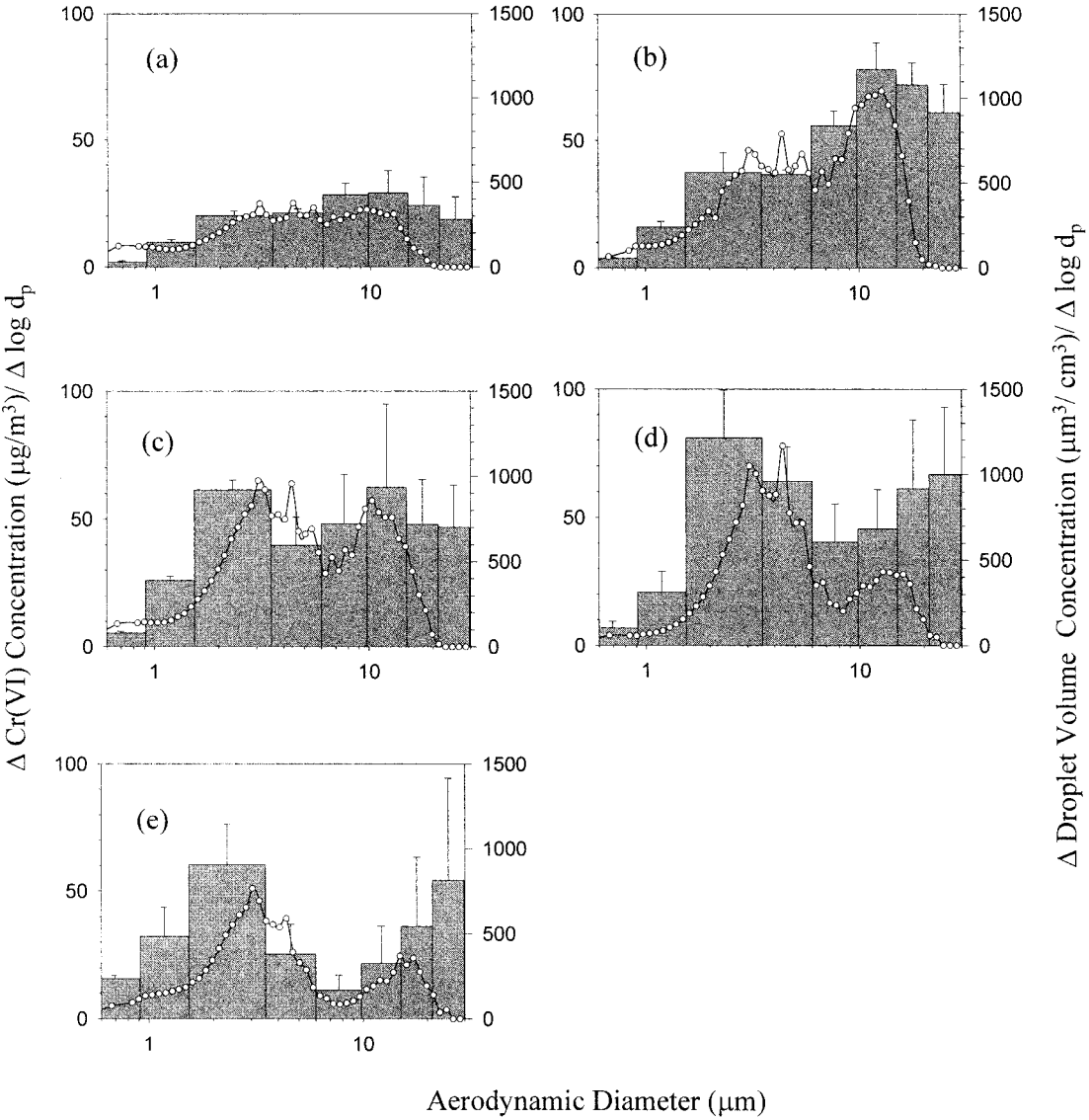

FIGURE 4. Airborne Cr(VI) mass distributions (shown as bars) in the droplets larger than 0.6 μm in aerodynamic diameter determined by a Marple personal cascade impactor for various CrO_3 concentrations: (a) 31.25 g / L, (b) 62.5 g / L, (c) 125 g / L, (d) 250 g / L, and (e) 375 g / L. The lines connecting open circles represent the corresponding droplet volume distributions.

tio, defined as the ratio of the Cr(VI) concentration in droplets to that of the bulk solution, is used to indicate the enrichment effect. The Cr(VI) concentration in droplets can be determined by dividing the Cr(VI) mass in droplets by the droplet volume calculated from droplet size data. In view of the decreasing sampling efficiency of the APS in the larger size range, the concentration ratios were calculated only for droplets in the aerodynamic size range of 1–10 μm.

Figure 5 shows that the concentration ratios decreased inversely with the concentration of CrO_3 in the bulk solution. This may be attributed to the process that Cr(VI) ions concentrate in a thin layer near the surface of the bubbles rising through the liquid and therefore enrich the film droplets formed by bursting bubbles (MacIntyre, 1970). This is because the enrichment of Cr(VI) in the droplets was mainly governed by the liquid surface tension. The Cr(VI) ions would be concentrated in the droplets when the liquid surface tension was lower than that of the solvent (water in this case).

Errors on the estimation of concentration ratios of Cr(VI) in droplets and in the bulk solution may result from the sizing errors of the Marple personal impactor and the APS. Possible changes in droplet size during sampling by both instruments is discussed below.

The Marple personal impactor was placed inside the chamber for all experiments and therefore the air temperature remained constant in the impactor. The air temperature may decrease as a result of aerodynamic cooling when the airflow in the

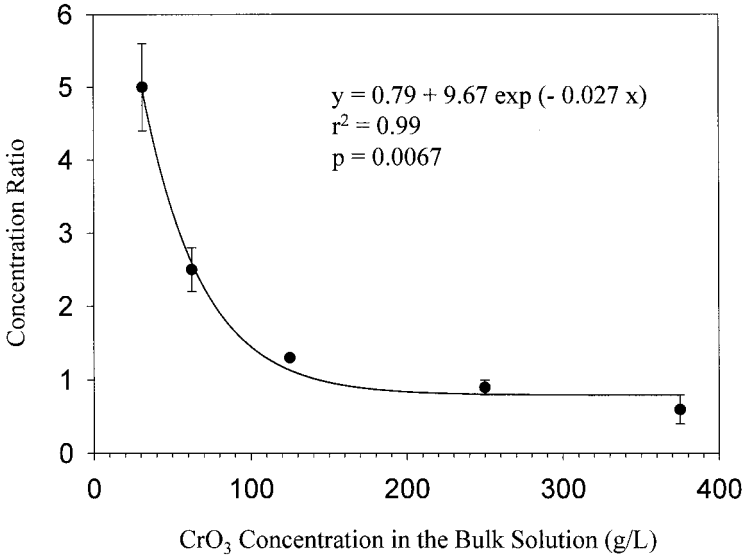

FIGURE 5. The enrichment of Cr(VI) in droplets of 1–10 μm in aerodynamic diameter for CrO_3 concentrations of 31.25, 62.5, 125, 250, and 375 g/L in the bulk solution. Each solid circle represents the mean of 3 replicates and an error bar represents one standard deviation.

impactor is accelerated to a fairly high velocity. However, even if the aerodynamic cooling effect is taken into account, the reduction of air temperature may take place only in the last 2 stages with cut-off diameters of 1 and 0.6 μm and is estimated to be about 0.2 and 0.6°C, respectively. During the residence time of droplets in each of the last 2 stages, which is about 70 and 30 μs, respectively, the growth in droplet diameter is $< 5\%$ in diameter.

As for the APS, it took only about 30 μs for the droplets to reach the laser beams from the inlet. A plastic tubing, 1.58 cm in inner diameter and 10 cm in length, connected the APS to the chamber. The residence time of droplets in this section was about 1 s. This may cause a reduction in air temperature. If it is assumed that the air temperature decreases from 37 to 28°C (the room temperature) at the end of the sampling tube and if the separating diameter between film and jet droplets is assumed to be about 7 μm, then the measured diameter would be about 8.6 μm as a result of growth due to condensation. This is quite consistent with the airborne Cr(VI) mass distributions shown in Figure 4, which were determined by the Marple personal impactor and showed a separating diameter at about the same size.

The studies of Van Grieken et al. (1974) and Piotrowicz et al. (1990) have demonstrated the enrichment of trace metal ions such as Cu, Fe, and Zn relative to Na from bursting bubbles. Those studies were, however, concerned with chemical fractionation by aerosolization of dilute solutions. Little is known about chemical fractionation by aerosolization of solutions of higher concentrations. The present study has focused on solutions of higher concentrations. The effect of electrolyte concentration on the enrichment of chromium in droplets from bursting bubbles was studied and data on the Cr(VI) enrichment with respect to the droplet size were obtained. The results should be useful in chromium emission control, health risk assessment, and understanding of chemical fractionation by aerosolization of concentrated solutions.

CONCLUSIONS

1. For CrO_3 concentrations in the range of 31.25–375 g/L and the airflow rate of 4 L/min, droplets generated from bursting of bubbles on the surface of electrolyte solutions were predominately in the submicrometer range. The CMDs of droplets were in the range of 0.15–0.18 μm.
2. The droplet volume distributions calculated from number distribution data were bimodal, indicating the presence of both film and jet droplets, which had a volume distribution mode of 3–4 μm and over 10 μm, respectively. As the CrO_3 concentration increased, the film droplet mode tended to shift toward smaller sizes, whereas the jet droplet mode tended to shift toward larger sizes.
3. The volume concentration of film droplets had a maximum at the electrolyte concentration of 125 g/L CrO_3 in the bulk solution. The Cr(VI) mass concentration of film droplets increased with increasing electrolyte concentration and reached a maximum, 52.9 $\mu g/m^3$, at the CrO_3 solution of 250 g/L in the bulk solution. For jet droplets, the maximum concentration for droplet volume and Cr(VI) both occurred at the CrO_3 concentration of 62.5 g/L in the bulk solution.
4. In the range of the electrolyte concentrations studied, the Cr(VI) concentration ratio between the droplets and the bulk solution declined from 5 to below unity with increasing CrO_3 concentration in the bulk solution.

This study was supported in part by Taiwan National Science Council Grant NSC 87-2211-E-002-015. Y. M. Kuo was supported by a stipend for graduate education awarded by the same grant of the Taiwan National Science Council during part of her Ph.D. study. The authors are grateful to Dr. C. C. Chen for his helpful suggestions in designing the experimental system and using the real-time aerosol instruments. The authors also wish to thank Dr. Paul Baron of the U.S. National Institute of Occupational Safety and Health for his comments on the manuscript.

References

Cipriano, R. J., and Blanchard, D. C. (1981). Bubble and Aerosol Spectra Produced by a Laboratory "Breaking Wave," *J. Geophys. Res.* 86(C9):8085–8092.

Exton, H. J., Latham, J., Park, P. M., Perry, S. J., Smith, M. H., and Allan, R. R. (1985). The Production and Dispersal of Marine Aerosol, *Q. J. R. Meterol. Soc.* 111:817–837.

Garner, F. H., Ellis, S. R. M., and Lacey, J. A. (1954). The Size Distribution and Entrainment of Droplets, *Trans. Instn. Chem. Engrs.* 32:222–235.

Hinds, W. C., and Kraske, G. (1986). Performance of PMS Model LAS-X Optical Particle Counter. *J. Aerosol Sci.* 17(1):67–72.

Hinds, W. C., and Kuo, T. L. (1990). Role of Liquid Properties on Droplet Formation by Bursting Bubbles. In Proceedings of the 3rd International Aerosol Conference, edited by S. Masuda and K. Takahashi. Pergamon Press, pp. 251–254.

Kinney, P. D. and Pui, D. Y. H. (1995). Inlet Efficiency Study for the TSI Aerodynamic Particle Sizer, *Part. Syst. Charact.* 12:188–193.

Lin, S. C., Tai, C. C., Chan, C. C., and Wang J. D. (1994). Nasal Septum Lesions Caused by Chromium Exposure Among Chromium Electroplating Workers, *Am. J. Ind. Med.* 26:221–228.

McCann, D. J., and Prince, R. G. H. (1971). Regimes of Bubbling at a Submerged Orifice, *Chemical Engineering Science* 26:1505–1512.

MacIntyre, F. (1970). Geochemical Fractionation During Mass Transfer from Sea to Air by Breaking Bubbles, *Tellus* 22:451–461.

Newitt, D. M., Dombrowski, N., and Knelan, F. H. (1954). Liquid Entrainment: The Mechanism of Drop Formation from Gas or Vapour Bubbles, *Trans. Inst. Chem. Eng.* 32:244–261.

Pilacinski, W., Pan, M. J., Szewczyk, K. W., Lehtimaki, M., and Willeke, K. (1990). Aerosol Released from Aerated Broths, *Biotechnol. and Bioeng.* 36:970–973.

Piotrowicz, S. R., Duce, R. A., Fasching, J. L., and Weisel, C. P. (1979). Bursting Bubbles and Their Effect on the Sea-to-Air Transport of Fe, Cu and Zn, *Marine Chemistry* 7:307–324.

Rader, D. J., Mondy, L. A., Brockmann, J. E., Lucero, D. A., and Rubow, K. L. (1991). Stage Response Calibration of the Mark III and Marple Personal Cascade Impactors, *Aerosol. Sci. Technol.* 14:365–379.

Resch, F., and Aftei, G. (1992). Submicron Film Drop Produced by Bubbles in Sea Water, *J. Geophys. Res.* 97(C3):3679–3683.

Rondia, D., and Closset, J. (1985). Aerosol Versus Solution Composition in Occupational Exposure, *Sci. Total Environ.* 46:107–112.

Rubow, K. L., Marple, V. A., Olin, J., and McCawley, M. A. (1987). A Personal Cascade Impactor: Design, Evaluation and Calibration, *Am. Ind. Hyg. Assoc. J.* 48(6):532–538.

Van Grieken, R. E., Johansson, T. B., and Winchester, J. W. (1974). Trace Metal Fractionation Effects Between Sea Water and Aerosols from Bubble Bursting, *Journal de Recherches Atmospheriques* 12:611–620.

Wangwongwatana, S., Scarpino, P. V., Willeke, K., and Baron, P. A. (1990). System for Characterizing Aerosols from Bubbling Liquids, *Aerosol Sci. Technol.* 13:297–307.

Washburn, E. W., West, C. J., Dorsey, N. E., and Ring, M. D. (1930). *International Critical Tables of Numerical Data, Physics, Chemistry and Technology.* Volume III. McGraw-Hill, New York.

Woolf, D. K., Bowyer, P. A., and Monahan, E. C. (1987). Discrimination Between the Film Drops and Jet Drops Produced by a Simulated Whitecap, *J. Geophys. Res.* 92(C5): 5142–5150.

Received July 20, 1998; accepted April 7, 1999.